

Mixing layer and coherent structures in compound channel flows: Effects of transverse flow, velocity ratio, and vertical confinement

Sébastien Proust, Joao N. Fernandes, Joao B. Leal, Nicolas Rivière, Yann Peltier

▶ **To cite this version:**

Sébastien Proust, Joao N. Fernandes, Joao B. Leal, Nicolas Rivière, Yann Peltier. Mixing layer and coherent structures in compound channel flows: Effects of transverse flow, velocity ratio, and vertical confinement. Water Resources Research, 2017, 53 (4), pp.3387-3406. 10.1002/2016WR019873 . hal-01724978

HAL Id: hal-01724978
https://hal.science/hal-01724978

Submitted on 16 May 2020

HAL is a multi-disciplinary open access archive for the deposit and dissemination of scientific research documents, whether they are published or not. The documents may come from teaching and research institutions in France or abroad, or from public or private research centers.

L'archive ouverte pluridisciplinaire **HAL**, est destinée au dépôt et à la diffusion de documents scientifiques de niveau recherche, publiés ou non, émanant des établissements d'enseignement et de recherche français ou étrangers, des laboratoires publics ou privés.

AGU PUBLICATIONS

Water Resources Research

RESEARCH ARTICLE
10.1002/2016WR019873

Key Points:
- Shear layer turbulence increases with local velocity ratio and with a decreasing vertical confinement of flow
- The existence of quasi-two-dimensional coherent structures is driven by velocity ratio and the direction and magnitude of transverse flow
- Coherent structures cannot develop if velocity ratio is lower than 0.3 and if a significant transverse flow toward the main channel occurs

Correspondence to:
S. Proust,
sebastien.proust@irstea.fr

Citation:
Proust, S., J. N. Fernandes, J. B. Leal, N. Rivière, and Y. Peltier (2017), Mixing layer and coherent structures in compound channel flows: Effects of transverse flow, velocity ratio, and vertical confinement, *Water Resour. Res.*, *53*, 3387–3406, doi:10.1002/2016WR019873.

Received 6 OCT 2016
Accepted 31 MAR 2017
Accepted article online 6 APR 2017
Published online 24 APR 2017

© 2017. American Geophysical Union. All Rights Reserved.

Mixing layer and coherent structures in compound channel flows: Effects of transverse flow, velocity ratio, and vertical confinement

S. Proust[1], J. N. Fernandes[2], J. B. Leal[3], N. Rivière[4], and Y. Peltier[5]

[1]IRSTEA, UR HHLY, Centre de Lyon-Villeurbanne, Villeurbanne, France, [2]Hydraulics and Environment Department, National Laboratory for Civil Engineering, Lisboa, Portugal, [3]Faculty of Engineering and Science, Universitetet i Agder, Grimstad, Norway, [4]Université de Lyon, INSA Lyon, CNRS, LMFA UMR 5509, Lyon, France, [5]Laboratoire d'hydraulique Saint-Venant, Ecole des Ponts, CEREMA, EDF R&D, UPE, Chatou, France

Abstract Turbulent mixing layers associated with streamwise uniform and nonuniform flows in compound channels (main channel with adjacent floodplains) are experimentally investigated. The experiments start with uniform flow conditions. The streamwise nonuniformity is then generated by imposing an imbalance in the upstream discharge distribution between main channel (MC) and floodplains (FPs), keeping the total discharge constant, which results in a transverse depth-averaged mean flow. This study first aims at assessing the effect of a transverse flow on the mixing layer and coherent structures that form at the MC/FP interfaces. A wide range of initial velocity ratio or dimensionless shear between MC and FP is tested. The study second aims at assessing the effect of this velocity ratio on the mixing layer, for a fixed vertical confinement of flow. The total discharge was then varied to quantify the confinement effect. The results show that, far from the inlet section, Reynolds-stresses increase with local velocity ratio for a fixed confinement and decrease with confinement for a fixed velocity ratio. It is also shown that, irrespective of confinement, the existence of quasi-two-dimensional coherent structures is driven by velocity ratio and the direction and magnitude of transverse flow. These structures cannot develop if velocity ratio is lower than 0.3 and if a strong transverse flow toward the MC occurs. In the latter case, the transverse flow is the predominant contribution to momentum exchange (compared with turbulent mixing and secondary currents), convex mean velocity profiles are observed, preventing the formation of quasi-two-dimensional structures.

Plain Language Summary Owing to the numerous sources of longitudinal nonuniformity along overflowing rivers (e.g., the change in floodplain land occupation), the understanding of overbank nonuniform flows in a compound open-channel (main channel and lateral floodplains) is of primary importance. Streamwise flow nonuniformity is characterized by a transverse flow across the river. At the interface between main channel (MC) and floodplain (FP), a mixing layer populated by turbulent vortices develops. When the flow is nonuniform, the mixing layer is strongly altered. These "nonuniform mixing layers" are encountered in several practical problems like mixing processes in rivers—e.g., sediments, nutrients, or pollutants transport from the MC to the FP—river restoration works, flood risk assessment studies. This paper presents an experimental investigation of nonuniform flows in compound channels, focusing on the mixing layer and the turbulent vortices. We assess the effects of the transverse flow on the turbulent vortices, as well as the effects of the MC/FP velocity ratio and of the vertical confinement of flow. The existence of quasi-two-dimensional vortices was found to be independent of the vertical confinement of flow (unlike uniform flows) but strongly driven by the velocity ratio and the direction and magnitude of the transverse flow.

1. Introduction

River floods often give rise to overbank flows in a compound open-channel (two-stage geometry with a main channel and lateral floodplains) that are nonuniform in the streamwise direction. Flow nonuniformity is characterized by longitudinal changes in flow depth and by a transverse depth-averaged mean flow,

herein termed "transverse flow," which is associated with a transverse net mass exchange. Several sources of flow nonuniformity can be found in nature, e.g., (i) longitudinal changes in the topography or/and in the hydraulic roughness of main channel and floodplains; (ii) backwater curve effects for subcritical flows; (iii) unbalanced discharge distribution between main channel and floodplains at the upstream boundary of a river reach; and (iv) flow unsteadiness. Therefore, the understanding of the mixing layer associated with nonuniform flows in a compound channel is of primary importance for practical problems like mixing processes of sediments or pollutants between the flows in the main channel (MC) and the floodplain (FP), river restoration works, flood risk assessment studies. We report here a laboratory investigation of these mixing layers subject to a transverse flow, when the latter is caused by an unbalanced upstream discharge distribution.

The first objective of this experimental work is to assess the effect of a transverse flow of variable magnitude and direction on the mixing layer and turbulent coherent structures that form at the MC/FP interfaces. The second objective is to assess the effect of a variable velocity ratio between subsections (MC and FPs) for a fixed vertical confinement of flow, which is not possible under uniform flow conditions. This is achieved by varying the upstream discharge distribution between subsections, keeping the total discharge constant. Lastly, varying this discharge enables the vertical confinement effect to be quantified for similar velocity ratio conditions.

Under uniform flow conditions, since the pioneering work of *Sellin* [1964], the transverse momentum exchange and the mixing processes between MC and FPs were comprehensively investigated in various laboratory flumes. *Knight and Shiono* [1990] and *Shiono and Knight* [1991] investigated how turbulent mixing and secondary currents contribute to the momentum exchange. As the relative flow depth D_r (ratio of the FP flow depth to that in the MC) rises, the velocity difference between subsections and shear layer turbulence decrease, while the secondary currents cells strengthen, especially in the MC [*Tominaga and Nezu*, 1991]. The shape of the lateral profiles of streamwise mean velocity, the number (one or two) of two-dimensional (2-D) coherent macrovortices at the MC/FP interfaces, and the mixing processes were also found to be a function of D_r [*Nezu et al*., 1999; *Stocchino and Brocchini*, 2010; *Stocchino et al*., 2011; *Besio et al*., 2012]. The role played by an abrupt transverse change in flow depth on the generation of 2-D macrovortices was analyzed by *Soldini et al*. [2004], following the approach of *Pratt* [1983]. The influence of rough FPs on the mixing layer was studied by *Fernandes et al*. [2014] and *Dupuis et al*. [2017a]. Here a question may be raised: what happens to those processes when the flow becomes nonuniform, i.e., in the presence of a transverse flow?

Most of the experimental works devoted to flow nonuniformity were carried out in nonprismatic compound geometries. The effect of the latter on the mean velocity profiles was investigated by *Elliot and Sellin* [1990] for skewed compound channels, by *Bousmar et al*. [2004] and *Proust et al*. [2006] for converging compound channels, and by *Bousmar et al*. [2006] and *Proust et al*. [2010] for enlarging compound channels. A detailed analysis of secondary currents and turbulent structures was performed by *Shiono and Muto* [1998] in compound meandering channels. The effect of a transverse flow on shear layer turbulence was evaluated by *Peltier et al*. [2013a] for rapidly varied flows caused by a transverse embankment located on the FP. In all these nonprismatic geometries, mass and momentum exchanges are strongly linked to the type of geometry studied. In addition, nonprismatic geometries simultaneously induce changes in transverse flow, velocity ratio, and vertical confinement of flow (quantified by D_r). Under these conditions, it is not possible to assess separately the effects of these three forcings on the mixing layer and coherent structures.

Putting aside the effect of nonprismatic geometries, we investigate here nonuniform flows in straight compound channels to focus on the basic mechanisms of interrelation between transverse flows and shear layer turbulence. Starting with uniform flow conditions, nonuniform flows are generated by imposing an imbalance in the upstream discharge distribution between subsections, keeping the total discharge constant. From a practical point of view, the study of unbalanced inflow conditions is interesting, because the velocity distribution is necessarily out of equilibrium at the upstream boundary of a compound reach [*Proust et al*., 2013]. For instance, an excess in FP inflow can be caused by narrowing FPs upstream of the studied reach [*Bousmar et al*., 2004], or by an abrupt FP contraction [*Proust et al*., 2006] in which a 34% flow excess was measured. Conversely, a deficit in FP inflow can be observed in enlarging FPs [*Bousmar et al*., 2006], ranging from −26% to −38% when compared to uniform flow conditions. Both an excess and a deficit in FP inflow

are investigated here, resulting in a transverse flow from FP to MC or from MC to FP, respectively. A wide range of velocity ratios FP/MC was tested. The total discharge was also varied to change flow confinement.

A transverse flow in a prismatic geometry was first investigated by *Proust* [2005] and *Bousmar et al*. [2005]. The focus was on the longitudinal evolution of the discharge distribution FP/MC. It was shown that a mass redistribution could occur over very large downstream distances, which increase with relative depth D_r and FP width B_f. The effect of a transverse flow on Reynolds-stresses was studied by *Proust et al*. [2013] for a single D_r-value ($D_r \sim 0.3$). It was shown that, for a fixed downstream position, and with an increasing transverse flow to the MC, the region of high values of Reynolds-stress was laterally and vertically stretched by the plunging flow into the MC. With a transverse flow to the FP, shear layer turbulence widely extends over the FP, with higher values of Reynolds-stress in the near-surface layer. Here we focus on the effect of the transverse flow on (1) the lateral distributions of streamwise mean velocity and turbulent quantities inside the mixing layer and (2) the development of quasi-2-D structures for various D_r-values. In addition, the contribution of transverse flow to the momentum exchange is quantified.

The effect of a velocity ratio between two parallel streams on turbulent mixing layers was examined in the case of free mixing layers [see e.g., *Yule*, 1972; *Winant and Browand*, 1974; *Oster and Wygnanski*, 1982]. It was shown that the near-field growing rate of the mixing layer was linked to the initial value of velocity ratio. Here we investigate the role played not only by the initial velocity ratio but also by the local velocity ratio further downstream, on shear layer turbulence and coherent structures. As velocity ratio was varied for a fixed total discharge, we can assess its effect irrespective of flow confinement.

The confinement effect on the mixing layer and coherent structures was investigated under uniform flow conditions, as previously mentioned. Under these conditions, the link between velocity ratio (or velocity difference) between subsections and relative depth D_r is unequivocal, and shear layer turbulence decreases with an increasing D_r-value. However, under nonuniform flow conditions, this link is no longer unequivocal. Here flows with the same velocity ratios but different confinements are compared. The confinement effect can thus be assessed regardless of the velocity ratio effect.

In section 2 of this paper, we present the two flumes in which the experiments were undertaken, along with the measuring techniques. In section 3, the flow conditions are detailed, focusing successively on the inflow conditions, the longitudinal development of flow depth and velocity ratio, and on typical cross-flow profiles of streamwise mean velocity and Reynolds-stress. Section 4 is dedicated to 2-D turbulence and the identification of quasi-2-D coherent structures. The effects of the three forcings (transverse flow, velocity ratio, and vertical confinement) on the mean flow, turbulent quantities, and coherent structures are analyzed in section 5. The paper concludes with the main findings of the study.

2. Experimental Apparatus and Measuring Techniques

2.1. The Two Flumes

The two flumes are located at the Laboratory of Fluid Mechanics and Acoustics (LMFA), Lyon, France, and at the National Laboratory of Civil Engineering (LNEC), Lisbon, Portugal. Their cross sections are depicted in Figure 1. The *x*, *y*, and *z* axes refer to the longitudinal (along the flume bottom), transverse, and vertical (normal to the flume bottom) directions, respectively. In this Cartesian reference frame, the system origin is defined as $x = 0$ at the inlet cross section; $y = 0$ at the right FP sidewall; and $z = 0$ at the MC bottom. The LMFA flume is PVC made, 8 m long and 1.2 m wide, with a longitudinal bottom slope S_0 of 1.8 mm/m. The

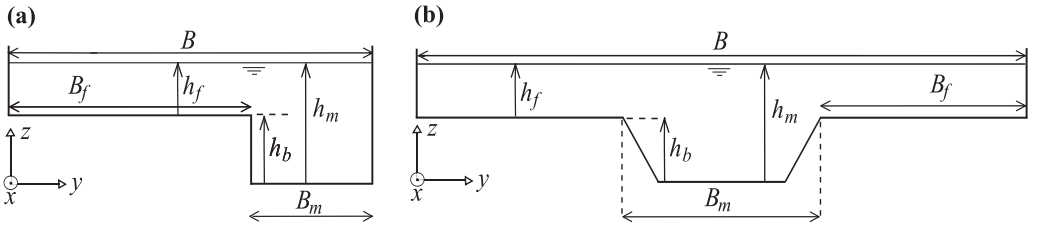


Figure 1. Sketches of the compound cross sections in the (a) LMFA flume and (b) LNEC flume. Subscripts "*f*" and "*m*" refer to floodplain and main channel, respectively. The height h_b is the bank full stage in the main channel.

cross section is asymmetrical, composed of a rectangular MC ($h_b = 5.3$ cm, $B_m = 39.5$ cm) and of one FP ($B_f = 80.5$ cm). The LNEC flume is made of polished concrete, 10 m long, 2 m wide, with a slope S_0 of 1.1 mm/m. The symmetrical cross section consists in a trapezoidal MC ($h_b = 10.0$ cm, $B_m = 60$ cm, bank-slope = 45°) and two FPs ($B_f = 70.0$ cm).

In both flumes, each subsection has an independent inlet tank and an independent pump, the subsection discharge being monitored by an electromagnetic flow meter. Originally designed to achieve uniform flow conditions over a short downstream distance [*Bousmar et al*., 2005], the independent tanks enable the change in the upstream discharge distribution MC/FP in order to obtain unbalanced inflow conditions (excess or deficit in FP inflow with respect to uniform flow conditions). This leads to a mass redistribution along the flume characterized by a transverse flow between subsections (see section 3). Upstream, the trailing edge of the splitter plates that separate two adjacent subsections is located at $x = 0.75$ m at LMFA, and at $x = 0.4$ m at LNEC. At the downstream end of the flumes, an independent tailgate is installed in each subsection.

2.2. Velocity and Water Level Measurements

In the coordinate system (x, y, z), the components of the instantaneous velocity, time-averaged velocity, and velocity fluctuations are denoted (u, v, w), (U, V, W), and (u', v', w'), respectively. In both flumes, the velocity was measured with a 10 MHz micro-side-looking ADV probe (Vectrino+). The sampling volume was a 7 mm long cylinder with 6 mm diameter. The acquisition duration was 180 s at a rate of 100 Hz. With 18,000 samples, the first and second statistical moments of turbulent statistics were converged. The number of samples was increased to 60,000 to compute the energy spectra and temporal autocorrelations functions of velocity fluctuations. The flow was seeded with 10 μm hollow glass spheres to get a signal-to-noise ratio higher than 20 dB as recommended by *McLelland and Nicholas* [2000]. The ADV data were despiked using the phase-space thresholding technique of *Goring and Nikora* [2002]. No additional filter was used. However, correlations lower than 70% were excluded from the time series. The errors of misalignment of the ADV probe with respect to the longitudinal direction were corrected according to *Peltier et al*. [2013b].

At LMFA, the measuring cross sections are located at downstream positions $x = 2.5$, 4.5, and 6.5 m for the flow cases with $D_r \sim 0.3$. Additional measurements were made along the MC/FP interface ($y/B_f = 1$), with a longitudinal spacing $\Delta x = 1$ m. For the cases with $D_r \sim 0.2$ and $D_r \sim 0.4$, the velocities were measured in one test section only, at $x = 4.5$ m. At LNEC, the measuring sections are located at $x = 1.1$, 3, 5, and 7.5 m, for the two investigated D_r-values (0.2 and 0.3). In both flumes, the typical lateral spacing Δy between measurements was 0.5–1 cm inside the mixing layer and 5–10 cm in the ambient streams. Along each vertical profile, at LMFA, eight measurements were made in the MC, and between one and four measurements in the FP for $D_r \sim 0.2$ and $D_r \sim 0.4$, respectively, and seven (resp. three) measurements were made in the MC (resp. FP) at LNEC.

The free surface elevation was measured with an ultrasonic sensor (Baumer UNDK20I69, standard error lower than 0.5 mm) at LMFA and with a point gauge (uncertainty of ±0.3 mm) at LNEC. At each x-position, 25 measurements were carried out across the section at LMFA, and 11 at LNEC.

Lastly, to get a better insight into the transverse development of the mixing layer, mean flow data collected by *Peltier et al*. [2013a] in the LMFA flume under uniform flow conditions were also used.

3. Flow Conditions of Test Cases

3.1. Inflow Conditions

The inflow conditions are given in Table 1. Starting with uniform flow conditions (flow depth and MC/FP discharge distribution both constant with respect to x axis), the upstream discharge distribution was then varied from one test to another, while keeping the total discharge Q unchanged. The variation in FP inflow with respect to uniform flow conditions, $(Q_f - Q_f^u)/Q_f^u$ ($x = 0$), is denoted $\Delta Q_f/Q_f^u$, where superscript u refers to uniform flow conditions. The same values of $\Delta Q_f/Q_f^u$ were investigated in both flumes, +19%, +38%, +53%, corresponding to excesses in the FP inflow, and −19% standing for a deficit. These unbalanced inflow conditions induced a transverse flow of variable magnitude and direction.

Table 1. Flow Conditions of Test Cases

Inflow Conditions ($x = 0$)			Longitudinal Average				Longitudinal Variations[a]			
Q (L/s)	Q_f/Q (%)	$\Delta Q_f/Q_f^u$ (%)	D_r	h_f (mm)	dh_f/dx ($\times$1000)	δ/h_f	U_{d1} (cm/s)	U_{d2} (cm/s)	λ	N
LMFA Flume										
17.3	11.2	−19		13.2	0.2	22.9	18.2	55.8	0.51	1.11
	13.8	0		13.9	0.0	15.8	20.1	55.0	0.46	1
	16.4	+19	0.2	14.4	−0.1	13.9	21.5	54.1	0.43	0.93
	19.0	+38		15.1	−0.2	11.7	23.7	52.6	0.38	0.83
	21.1	+53		15.4	−0.3	11.4	24.3	52.7	0.37	0.80
24.7	20.6	−19		21.8	0.3	8.2	30.2–30.4	72.0–66.4	0.41–0.37	1.4–1.28
	25.4	0		23.2	0.0	5.9	33.4–34.6	58.9–62.6	0.28–0.29	0.97–1.00
	30.2	+19	0.3	23.9	−0.1	4.3	38.2–36.8	56.0–61.8	0.19–0.25	0.66–0.86
	35.0	+38		24.8	−0.4	2.7	41.2–40.1	53.0–59.8	0.13–0.20	0.45–0.69
	38.8	+53		24.9	−0.6	3.0	43.1–41.8	51.4–60.3	0.09–0.18	0.31–0.62
36.3	31.5	−19		36.0	0.4	6.5	42.9	75.0	0.27	1.59
	38.8	0		36.9	0.0	2.6	47.9	67.8	0.17	1.00
	46.2	+19	0.4	37.0	−0.7	2.0	51.7	62.2	0.09	0.53
	53.6	+38		37.3	−1.0	N.D.[b]	N.D.	N.D.	N.D.	N.D.
	59.4	+53		37.3	−0.9	N.D.	N.D.	N.D.	N.D.	N.D.
LNEC Flume										
53.4	17.0	−19		21.3	0.3	10.5	33.1–31.3	73.4–69.5	0.38–0.38	1.09–1.09
	21.0	0		22.4	0	10.2	35.1–35.1	67.1–72.6	0.31–0.35	0.89–1.00
	24.9	+19	0.2	23.9	−0.6	8.0	35.3–35.1	65.2–71.4	0.30–0.34	0.86–0.97
	29.0	+38		24.4	−0.6	7.2	38.6–35.0	62.6–70.9	0.24–0.34	0.69–0.97
	32.0	+53		25.3	−0.7	6.9	42.6–37.0	59.9–69.9	0.17–0.31	0.49–0.89
80.6	26.6	−19		38.6	0.2	5.9	40.6–40.1	82.9–79.1	0.34–0.33	1.36–1.32
	32.8	0		40.1	0.0	4.9	46.9–45.1	81.5–75.5	0.27–0.25	1.08–1.00
	39.0	+19	0.3	41.0	−0.3	5.1	50.9–47.9	74.5–71.5	0.19–0.20	0.76–0.80
	45.2	+38		41.6	−0.5	4.8	N.D. to 54.4	N.D. to 70.1	N.D. to 0.13	N.D. to 0.52
	50.1	+53		41.9	−0.7	N.D.	N.D. to N.D.	N.D. to N.D.	N.D. to N.D.	N.D to N.D.

[a]Variations between the most upstream and downstream measuring sections. At LMFA, for $Q = 17.3$ and 36.3 L/s, velocity measurements in one cross section only, at downstream distance $x = 4.5$ m.
[b]N.D.: not defined.

Note that, for each Q-value, five cases are subject to the same confinement or topographical forcing (similar relative depth D_r). By contrast, velocity ratio significantly varies from one case to another (section 3.2). This protocol is original in comparison with the previous uniform compound channel flow experiments, since in the present study, there is no longer an unequivocal link between D_r and velocity ratio, as detailed in section 3.3.

3.2. Flow Depth and Velocity Ratio

Figure 2 shows, for 15 flow cases, the average flow depth in the FP, h_f, and velocity ratio, λ, against the longitudinal position x, which is normalized by B_f as proposed by *Bousmar et al.* [2005]. Also known as dimensionless shear, velocity ratio is defined as

$$\lambda(x) = \frac{U_{d2} - U_{d1}}{U_{d2} + U_{d1}}(x) \tag{1}$$

where U_{d1} and U_{d2} are the streamwise depth-averaged velocities of the two ambient streams outside the mixing layer. Note that, for free mixing layers, the parameter 2λ quantifies the relative magnitude of the velocity difference between the two ambient streams (also termed "destabilizing shear") with respect to the convection velocity of turbulent structures [see e.g., *Huerre and Rossi*, 1998].

The values of h_f, U_{d1}, U_{d2}, and λ are given in Table 1 for the whole data set. We also report the values of the nonuniformity parameter N, defined at a given x-position as

$$N(x) = \frac{\lambda(x)}{\lambda^u} \tag{2}$$

where λ^u is the velocity ratio measured in the last measuring section for the uniform flow of same total discharge Q.

In Figure 2, the uniform flows feature constant flow depth in the second half of the flumes. The nonuniform cases feature average streamwise flow depth gradients dh_f/dx of the order of magnitude of the bottom

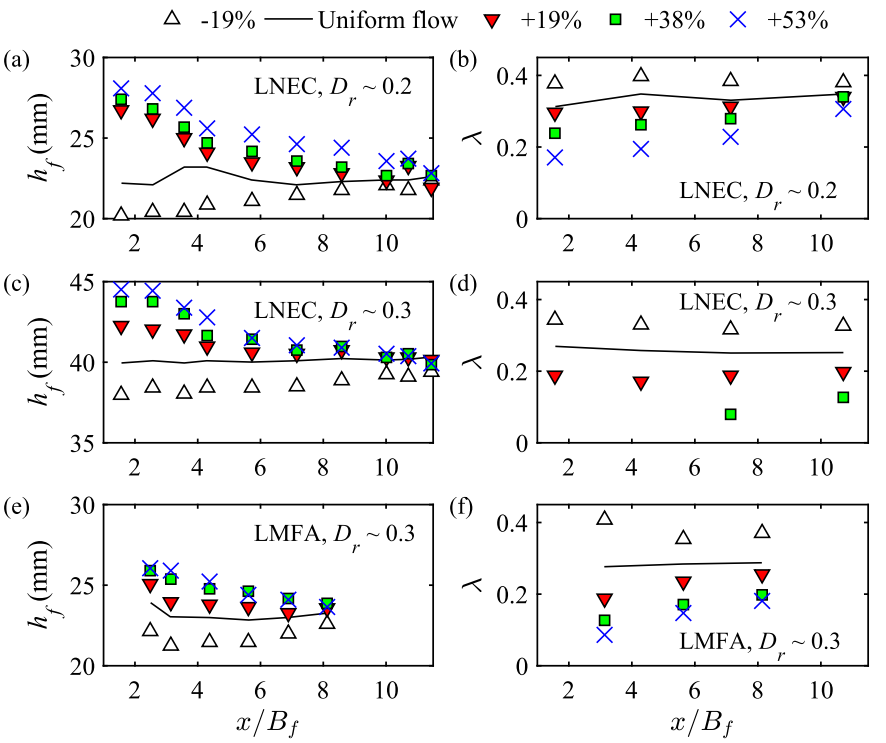


Figure 2. Floodplain flow depth h_f and velocity ratio λ against downstream distance x/B_f. Uniform flows and cases with a FP inflow $\Delta Q_f/Q_f^u = -19\%$, $+19\%$, $+38\%$, and $+53\%$.

slope (from 0.4×10^{-3} to -1×10^{-3}, see Table 1). In the most downstream measuring section, the flow depth h_f is very close to the uniform flow value, h_f^u. By contrast, velocity ratio λ is close to the uniform value λ^u for only two cases, $+19\%$ and $+38\%$ with $D_r \sim 0.2$ at LNEC (see Figure 2b) for which $N = 0.97$ in Table 1. For the other nonuniform cases, the N-values in the last measuring section can strongly differ from 1 (Table 1). For instance, for the cases with $D_r \sim 0.3$ at LMFA (Figures 2e and 2f), $N \in$ [0.62 to 1.28] at $x/B_f = 8.1$ while confinement is very similar ($h_f \in$ [22 to 24 mm]).

As a result, for the vast majority of cases, the flow depth tends toward equilibrium over a shorter longitudinal distance than the mean flow velocity, as previously shown by *Bousmar et al.* [2005]. As velocity ratio evolves slowly in comparison with flow depth, the velocity ratio imposed upstream will play a significant role on the flow structure further downstream.

Bousmar et al. [2005] actually showed that, when the upstream discharge distribution is out of equilibrium, the length required for reaching mean flow uniformity increases with D_r. The data in Table 1 are consistent with this result. For a given disequilibrium $\Delta Q_f/Q_f^u$, the difference between $N(x)$ and 1 in the last measuring section increases with D_r. This is due to the fact that, for a given value of $\Delta Q_f/Q_f^u$, the amount of water to be transferred to reach uniformity increases with total discharge Q, i.e., with D_r. For instance, at LMFA with $\Delta Q_f/Q_f^u = -19\%$, $(Q_f - Q_f^u)$ $(x = 0) = -0.45$ L/s, -1.19 L/s, and -1.80 L/s for $D_r = 0.2$, 0.3, and 0.4, respectively.

Lastly, all flows are subcritical with Froude numbers in the two ambient streams $F_1 = U_{d1}/(g\ h_f)^{0.5}$ and $F_2 = U_{d2}/(g\ h_m)^{0.5}$ ranging from 0.51 to 0.87 and from 0.60 to 0.86, respectively at LMFA, and from 0.66 to 0.87 and from 0.53 to 0.71, respectively, at LNEC. The Reynolds numbers $R_{e1} = h_f\ U_{d1}/\nu$ and $R_{e2} = h_m\ U_{d2}/\nu$ are in the range [0.2×10^4 to 2×10^4] and [3×10^4 to 6×10^4] respectively, at LMFA, while $R_{e1} \in$ [0.7×10^4 to 2×10^4] and $R_{e2} \in$ [8×10^4 to 11×10^4], at LNEC.

3.3. Typical Profiles of Depth-Averaged Velocity and Reynolds-Stress

Figure 3 shows transverse profiles of depth-averaged streamwise velocity U_d and depth-averaged Reynolds-stress $-\overline{(u'v')}_d$ ($^-$ refers to time averaging and subscript d to depth averaging) for 15 flow cases. As proposed by *Stocchino and Brocchini* [2010] and *Dupuis et al.* [2017b], these quantities are normalized by the interfacial velocity U_{int} (measured at $y/B_f = 1$).

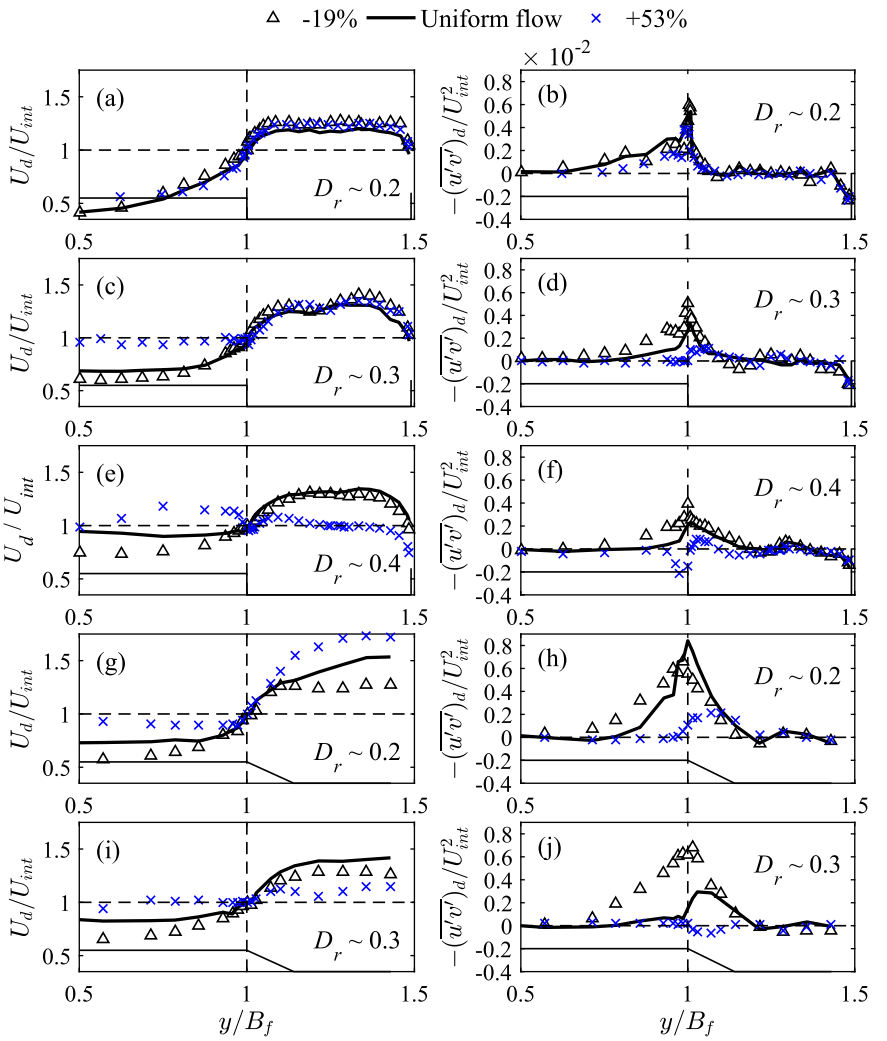


Figure 3. Depth-averaged streamwise velocity U_d/U_{int} and depth-averaged Reynolds-stress $-\left(\overline{u'v'}\right)_d/U_{int}^2$ against lateral distance y/B_f for various relative flow depths D_r. (a–f) LMFA, downstream distance $x/B_f = 5.6$ and (g–j) LNEC, $x/B_f = 10.7$ (right-hand half profiles).

Under uniform flow conditions, *Nezu et al.* [1999] and *Stocchino and Brocchini* [2010] classified mean velocity profiles depending on the D_r-value. When $D_r < 0.33$ (shallow flow regime), velocity profile is monotonic with a strong gradient near the interface. As shown in Figures 3a, 3c, 3g, and 3i, the uniform flows with $D_r \sim 0.2$ and 0.3 in both flumes have these features. Note that the uniform flow with $D_r \sim 0.4$ at LMFA appears to also belong to this category (Figure 3e). The monotonic profile is related to 2-D macrovortices that rotate clockwise within the right-hand shear layer [*Stocchino and Brocchini*, 2010]. When $0.33 < D_r < 0.5$ (intermediate flow regime), *Stocchino and Brocchini* [2010] observed that velocity profiles were nonmonotonic with a velocity dip near the interface. These authors and *Nezu et al.* [1999] both observed that the dip can be ascribed to a Karman alley with counterrotating macrovortices in the interfacial region.

When the flow is nonuniform, the link between the shape of mean velocity profile and D_r is no longer unequivocal. First, this can be clearly seen in Figure 3e for flow cases with $D_r \sim 0.4$ at LMFA. The velocity profile is monotonic for case −19%, and nonmonotonic with a velocity dip near the interface for case +53%, despite the rather similar flow confinement ($h_f = 36.0$ and 37.3 mm, respectively, see Table 1). This results in very different Reynolds-stress distributions (Figure 3f). Second, for a D_r-value ranging from 0.2 to 0.4, all cases −19% feature monotonic velocity profiles (Figures 3a, 3c, 3e, 3g, and 3i) with comparable shapes of Reynolds-stress distributions (Figures 3b, 3d, 3f, 3h, and 3j).

The variation in the velocity profile shape, irrespective of the D_r-value, is due to the effects on the streamwise mean flow of (i) a variable velocity ratio and (ii) a transverse flow of variable magnitude and direction, as it will be shown in section 5.

4. Quasi-2-D Coherent Structures

4.1. 2-D Turbulence

In the present study, we investigate how the three forcings (velocity ratio, transverse flow, and flow confinement) affect shear layer turbulence and coherent structures, with a focus on the conditions of existence of 2-D coherent structures. Their identification is based on previous works dealing with 2-D-turbulence. Two types of 2-D turbulence must be distinguished:

1. The first type is a purely 2-D turbulence, based on the 2-D Navier-Stokes equations and on the theory of *Kraichnan* [1967]. This 2-D isotropic turbulence, forced at a wave number k_i, is a freely decaying turbulence featuring an energy spectrum with a double cascade, as schematized in *Lesieur* [1997, Figure 8−3]. According to *Kraichnan* [1967], the $k^{-5/3}$ spectrum is the spectrum of a 2-D turbulence with an inverse energy cascade, from large to small k-wave numbers, i.e., from small to large scales, while the k^{-3} range is a forward 2-D enstrophy (half the square of vorticity) cascade in the inertial range (high k-values) in which enstrophy is transferred from large to small scales. For this type of turbulence, there is no vortex stretching [*Lindborg*, 1999]. This 2-D turbulence was experimentally observed, among others, by *Rutgers* [1998] in flowing soap films.
2. The second type is a quasi-2-D turbulence, for which vortex stretching can occur and quasi-2-D and three-dimensional (3-D) structures can coexist. It was observed by *Dracos et al*. [1992] in shallow turbulent jets, by *Uijttewaal and Booij* [2000] in free surface mixing layers, and by *Stocchino and Brocchini* [2010] in a compound channel. The development of quasi-2-D turbulence is also characterized by an enstrophy cascade with a k^{-3} spectrum. However, conversely to the first type, this cascade is located in the middle range of k, where an energy peak is also observed. In the inertial range, a $k^{-5/3}$ forward energy cascade like in 3-D turbulence is observed.

4.2. Identification of Structures

Following the previously cited works, we identified the presence of quasi-2-D structures by computing the energy spectra of turbulence and by seeking for an enstrophy cascade with a k^{-3} spectrum. Figure 4a shows the power density spectra S_{yy} of transverse velocity fluctuation v' against the k-wave number (equals to $2\pi f/U$, where f is the signal frequency), at the MC/FP interface for the five cases with $D_r \sim 0.2$ at LNEC. For case −19% and uniform flow, a peak in S_{yy} can be observed in the middle range of k with a −3 slope on the high k-wave number side. Following *Dracos et al*. [1992] and *Uijttewaal and Booij* [2000], this can be ascribed to the development of quasi-2-D structures.

The coherence of these quasi-2-D structures was quantified from the temporal autocorrelation function R_{yy} of velocity fluctuation v', as displayed in Figure 4b. This figure shows that the turbulent structures of flow

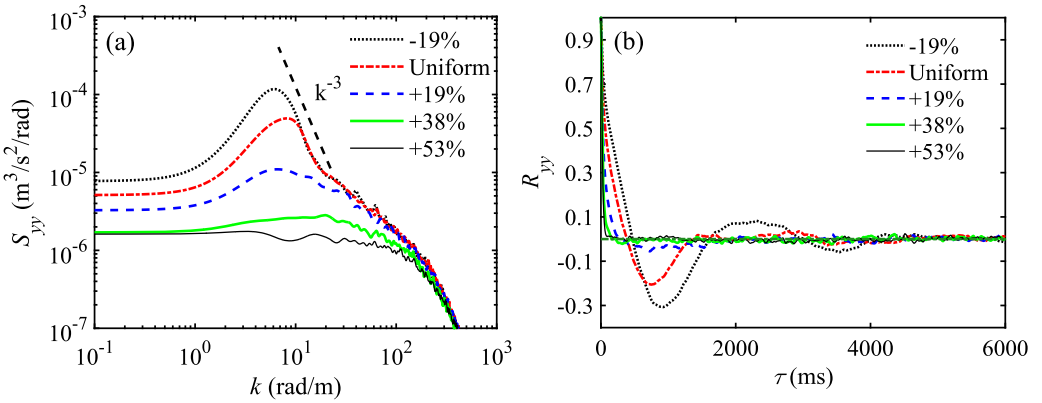


Figure 4. (a) Power density spectra S_{yy} and (b) temporal autocorrelation function R_{yy} of velocity fluctuation v'. Measurements at $x/B_f = 10.7$, at $y/B_f = 1$, and at 40% of the FP flow depth. LNEC, cases with relative depth $D_r \sim 0.2$.

case −19% and uniform flow are coherent over a much longer duration than those of cases +19%, +38%, and +53%.

4.3. Influence of Quasi-2-D Structures on Mixing Layer Width

Figure 5 shows S_{yy} and R_{yy} along the interface for cases −19% and +19% with $D_r \sim 0.3$ at LMFA. A measurement outside the mixing layer (denoted "Outside ML") at $x/B_f = 8.1$ and at $y/B_f = 0.25$ is also plotted for comparison.

Case −19% features a development of quasi-2-D-structures along the whole measuring domain (Figure 5a). Inside the mixing layer, the levels of S_{yy} are one order of magnitude higher than the ones outside the mixing layer. The autocorrelation function R_{yy} shows that the temporal coherence of the quasi-2-D structures also increases in the longitudinal direction (Figure 5b). Note that, outside the mixing layer, the S_{yy} curve features also a small peak in the middle range of k. This may correspond to quasi-2-D structures coming from upstream, which have very little coherence (see R_{yy} curve "Outside ML").

With case +19% (Figures 5c and 5d), the quasi-2-D coherent structures vanish at the interface, with levels of S_{yy} close to the ones measured outside the mixing layer. The same results hold at a given x-station, when exploring various y-positions on both sides of the interface (not shown here).

As quasi-2-D structures makes easier the momentum transfer by turbulent mixing between the flows in the MC and FP, mixing layer width will be strongly linked to their existence. Adapting the notations used for free mixing layers [*Pope*, 2000] to our vertically confined mixing layers, mixing layer width is defined as

$$\delta = y_{0.9} - y_{0.1} \tag{3}$$

with $U_d(y_\alpha) = U_{d1} + \alpha(U_{d2} - U_{d1})$ for $0 < \alpha < 1$.

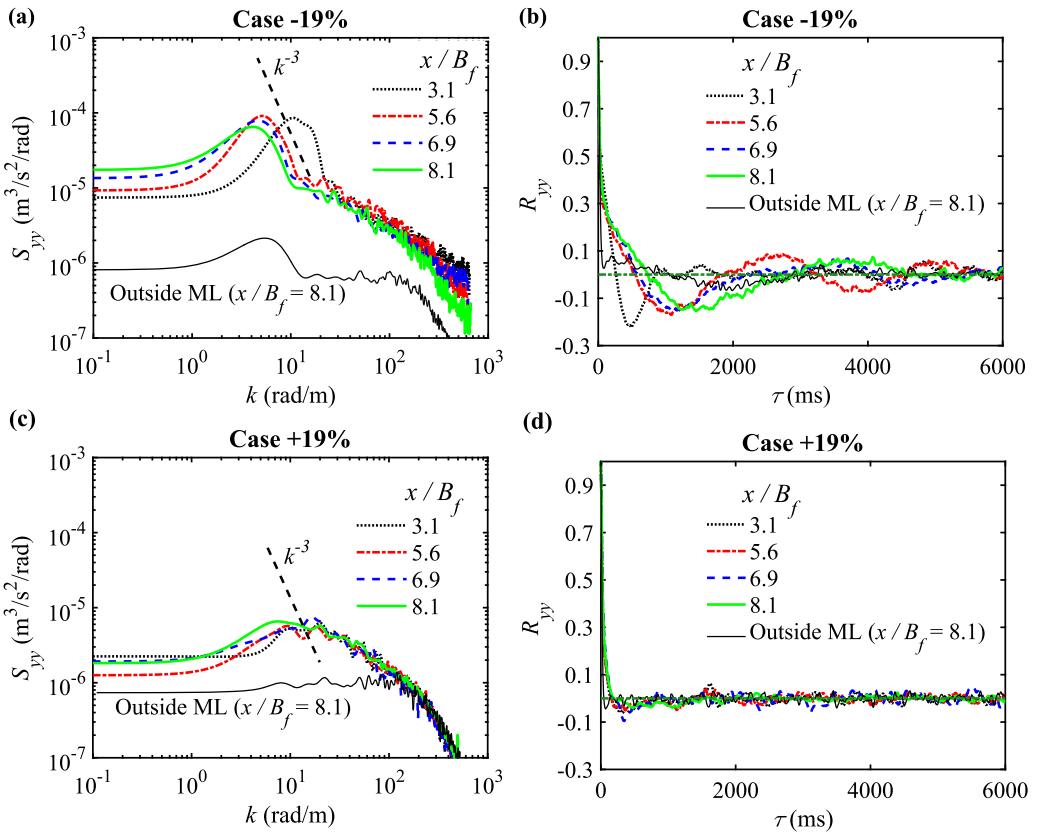


Figure 5. Power density spectra S_{yy}, and temporal autocorrelation function R_{yy}, of lateral velocity fluctuation v' along the interface ($y/B_f = 1$) at 40% of the FP flow depth, for $3.1 \leq x/B_f \leq 8.1$. LMFA, relative depth $D_r \sim 0.3$: (a, b) case −19% and (c, d) case +19%.

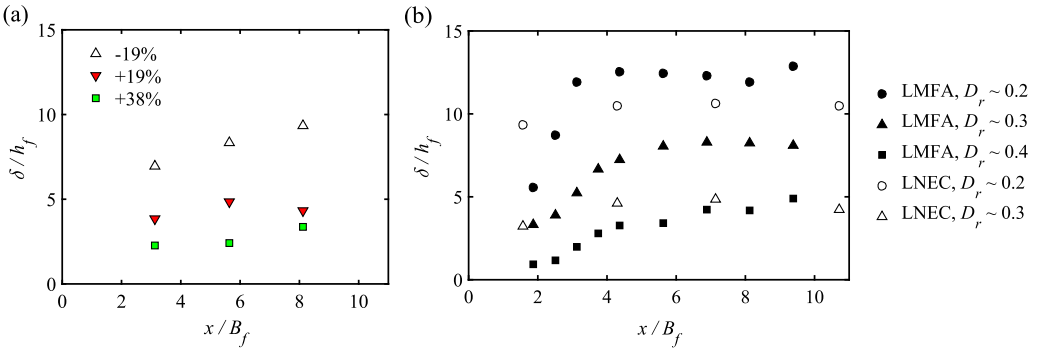


Figure 6. Mixing layer width-to-depth-ratio δ/h_f against downstream distance x/B_f for (a) nonuniform cases −19%, +19%, and +38% with $D_r \sim 0.3$ at LMFA and (b) uniform flows at LMFA (data from *Peltier et al.* [2013a]).

Figure 6a shows the width δ scaled by the FP flow depth, as a function of downstream distance for cases with $D_r \sim 0.3$ at LMFA. For case −19%, the development of quasi-2-D coherent structures along the flume (Figures 5a and 5b) is associated with a large and increasing width δ (Figure 6a). By contrast, for case +19%, the absence of quasi-2-D structures (Figures 5c and 5d) does not promote the transverse development of shear layer turbulence, resulting in a small and fairly constant δ-value (Figure 6a).

It should be noticed that, for case −19%, the value of k for which S_{yy} exhibits a peak is of the order of some units (Figure 5a). It corresponds to a streamwise integral length scale Λ_x of quasi-2-D structures that is several times higher than δ. This is not surprising as a ratio $\Lambda_x/\delta \sim 3.5$ was measured by *Uijttewaal and Booij* [2000] for shallow mixing layers, $\Lambda_x/\delta \sim 3$ at the boundary of recirculating flow area [*Han et al.*, 2016], and $\Lambda_x/\delta \sim 4$–8 in compound channels with rough FP [*Dupuis et al.*, 2017a].

5. Effect of the Three Forcings

5.1. Transverse Flow

In this section, we first investigate the three sources of transverse exchange of streamwise momentum: turbulent mixing, secondary currents, and transverse flow. We second analyze the effect of the transverse flow on the cross-sectional distribution of Reynolds-stress. Lastly, we assess the interrelation mechanisms between transverse flow, the shape of streamwise velocity profiles, and the existence of quasi-2-D structures.

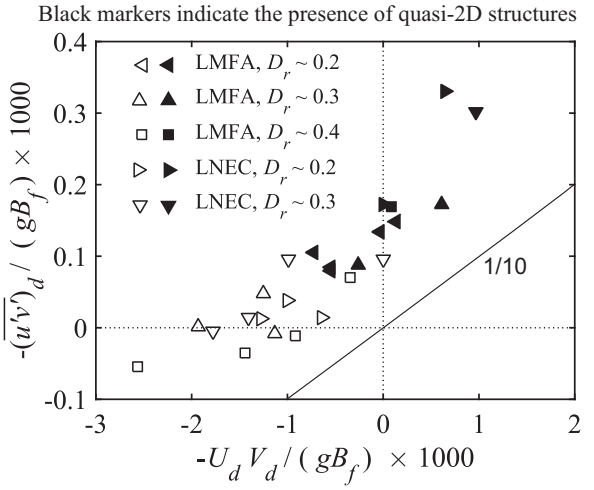


Figure 7. Transverse momentum exchange by turbulent mixing $-\overline{(u'v')}_d/(gBf)$, versus momentum exchange by transverse flow $-U_dV_d/(gB_f)$. Measurements at the interface ($y/B_f = 1$) and at $x/B_f = 5.6$ and 7.1 at LMFA and LNEC, respectively.

5.1.1. Transverse Momentum Exchange

As the estimate of the transverse momentum exchange has been a constant preoccupation in the literature of uniform compound channel flows, we examine here this momentum flux under nonuniform flow conditions. We use depth-averaged values as commonly done for uniform flows [*Shiono and Knight*, 1991]. The depth-averaged and time-averaged transverse exchange of streamwise momentum has three contributions [*Proust et al.*, 2013]:

$$\overline{\frac{1}{h}\int_0^h -\rho uv dz} = -\rho\overline{(u'v')}_d - \rho U_d V_d - \rho[U(V-V_d)]_d \quad (4)$$

where h is local flow depth and ρ is fluid density. The first contribution is the depth-averaged Reynolds-stress, the term $-\rho U_d V_d$ is the momentum transfer by the transverse

flow, and the term $-\rho[U(V-V_d)]_d$ is the depth-averaged momentum transfer by the secondary currents.

First, it should be reminded that transverse velocity V_d quantifies the transverse net mass exchange over the water column, and is equal to zero when the flow is uniform. Second, the estimate of the secondary current term $-\rho[U(V-V_d)]_d$ requires a sufficient number of measurements over the depth. Hence, it cannot be evaluated for the shallowest flow cases.

In a first step, the secondary currents contribution will not be considered to compare the contributions of $-\rho\overline{(u'v')}_d$ and $-\rho U_d V_d$ to the momentum flux for the whole data set. Focusing on the momentum exchange at the MC/FP interface (at $y/B_f = 1$), these two terms have been normalized by $\rho g B_f$, relying on the 1-D momentum conservation equation formulated in one FP [*Proust et al.*, 2009], which reads in the right-hand FP

$$S_{ff} = S_0 - \frac{dh_f}{dx} - \frac{1}{gh_f}\frac{d\left(h_f U_f^2\right)}{dx} + \frac{-\overline{(u'v')}_d|_{y/B_f=1}}{gB_f} - \frac{U_d V_d|_{y/B_f=1}}{gB_f} \tag{5}$$

where S_{ff} is the FP friction slope and U_f is the FP average velocity.

The terms $-\overline{(u'v')}_d/(gB_f)$ and $-U_d V_d/(gB_f)$ are plotted in Figure 7. The variation range of $-\overline{(u'v')}_d/(gB_f)$ is one order of magnitude lower than the range of $-U_d V_d/(gB_f)$, highlighting the predominant role played by the transverse flow in the momentum transfer. Figure 7 also shows that with an increasing transverse flow toward the MC ($V_d > 0$ and $-U_d V_d < 0$), $-\overline{(u'v')}_d/(gB_f)$ becomes quickly negligible with respect to $-U_d V_d/(gB_f)$. By contrast, with a transverse flow to the FP ($V_d < 0$ and $-U_d V_d > 0$), turbulent mixing and transverse flow can both contribute to momentum transfer.

In a second step, accounting for secondary currents, the three contributions to momentum flux in equation (4) were evaluated across the total section for the cases with the highest relative depth ($D_r \sim 0.4$ at LMFA). They are plotted in Figure 8 (after being normalized by $\rho g B_f$). Figure 8a shows that the momentum exchange by secondary currents and turbulent mixing can be of the same order of magnitude. When comparing these two contributions with $-U_d V_d/(gB_f)$ in Figure 8b, the results differ depending on the direction of transverse flow. With a transverse flow to the FP (case −19%), the three sources of momentum can contribute to momentum exchange, especially near the interface (as observed by *Vermaas et al.* [2011] in a shallow mixing layer with a lateral roughness transition). With a transverse flow to the MC (case +53%), momentum transfer is essentially driven by the transverse flow.

5.1.2. Cross-Sectional Distribution of Reynolds-Stress

The distribution of Reynolds-stress is displayed in Figure 9 at various *x*-positions for cases +19% and −19% with $D_r \sim 0.3$ at LNEC. Reynolds-stress is normalized by the velocity difference between the two ambient streams, $U_s = U_{d2} - U_{d1}$, similarly to free mixing layers.

Figure 9 shows that the impact of transverse flow on the transverse development of turbulent quantities is dependent upon its direction. With a transverse flow to the MC (Figure 9a), shear layer turbulence is essentially contained in the MC. This is caused by the "mechanical" effect of transverse flow on turbulent

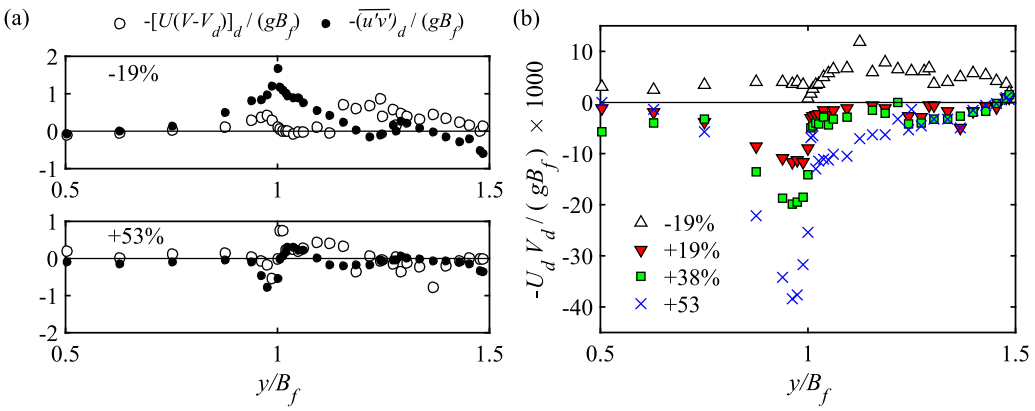


Figure 8. Transverse momentum exchange by (a) the secondary currents $-[U(V-V_d)]_d/(gB_f)$ and turbulent mixing $-\overline{(u'v')}_d/(gBf)$, and by (b) the transverse flow $-U_d V_d/(gB_f)$. LMFA, nonuniform cases with $D_r \sim 0.4$, at $x/B_f = 5.6$.

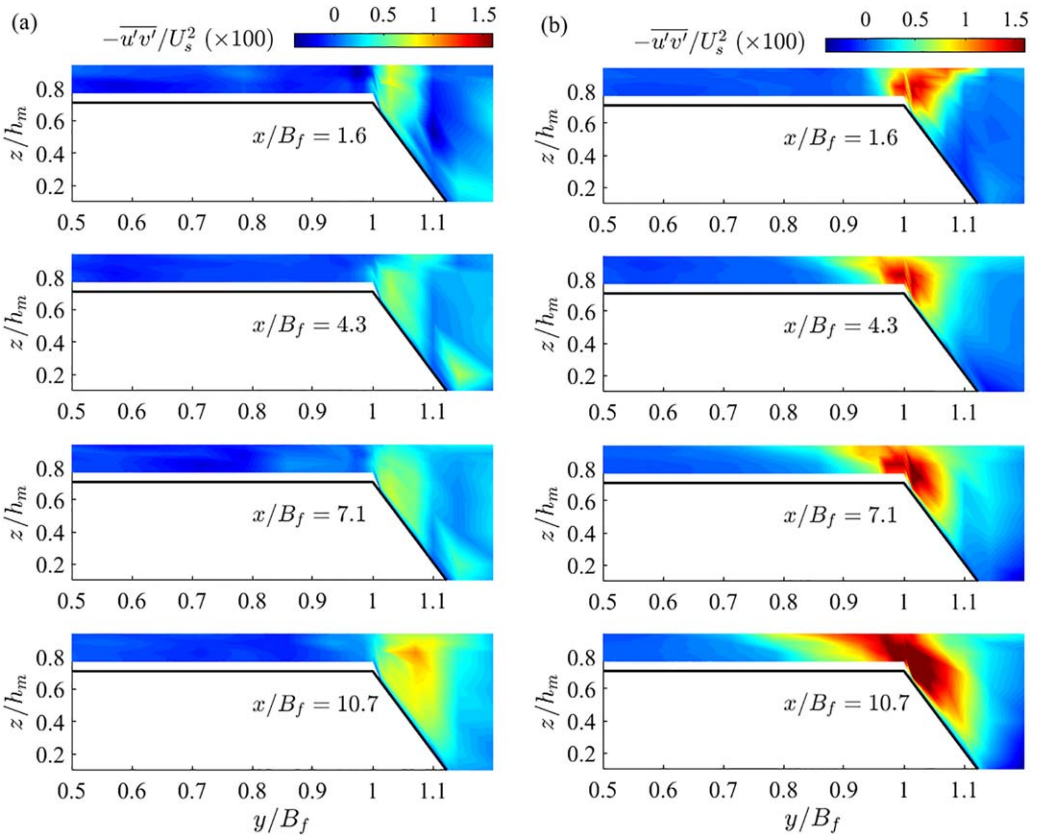


Figure 9. Cross-sectional distribution of dimensionless Reynolds-stress $-\overline{u'v'}/U_s^2$ (×100) at various downstream positions x/B_f. LNEC, $D_r \sim 0.3$, cases (a) +19% and (b) −19%.

structures: the transverse depth-averaged velocity V_d, which is maximum at the MC/FP interface [*Proust et al.*, 2013] acts as a vertical screen that prevents shear layer turbulence from developing over the FP. This has an important practical consequence for field studies, since the exchange by turbulent mixing of sediments, nutrients or pollutants from MC to FP is not possible in this case. By contrast, with a transverse flow to the FP (Figure 9b), turbulence can widely develop over the FP further downstream.

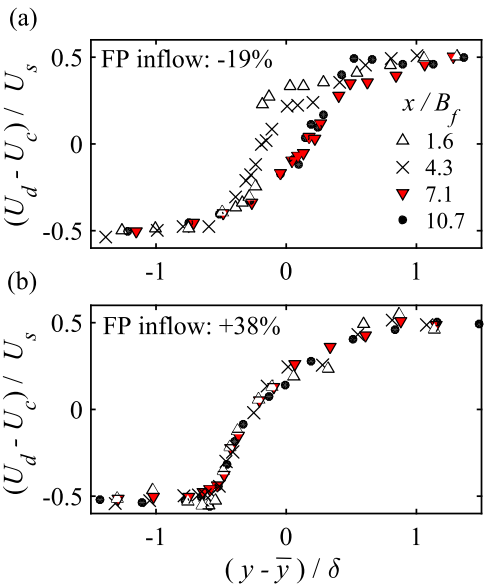


Figure 10. Dimensionless depth-averaged streamwise velocity, $(U_d - U_c)/U_s$, across the mixing layer. Cases (a) −19% and (b) +38% with $D_r \sim 0.2$ at LNEC.

5.1.3. Convex Versus Inflection Point Velocity Profile

The five flow cases with $D_r \sim 0.2$ at LNEC are of particular interest, since both flow depth and velocity ratio λ are close to equilibrium in the last measuring section (Figure 2). The characteristics of these flows were investigated inside the mixing layer, by using the dimensionless transverse coordinate, $(y-\overline{y})/\delta$, where $\overline{y}$ is the centerline position in the mixing layer:

$$\overline{y} = (y_{0.9} + y_{0.1})/2 \quad (6)$$

Figure 10 shows the dimensionless depth-averaged streamwise velocity, $(U_d - U_c)/U_s$, as a function of $(y-\overline{y})/\delta$ for cases −19% and +38%, where U_c is the average velocity across the mixing layer $[(U_{d2} + U_{d1})/2]$. Figure 11 shows the dimensionless depth-averaged

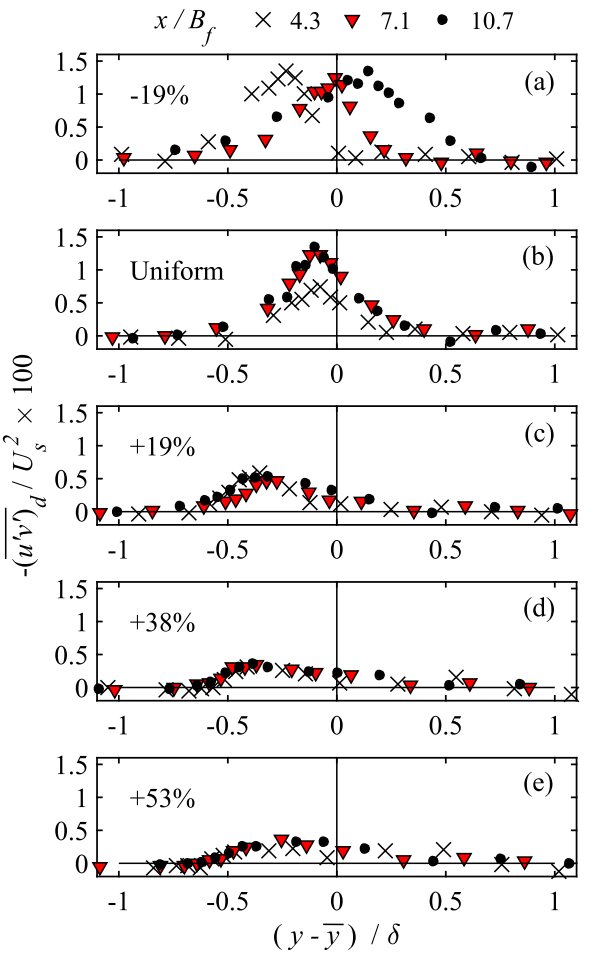


Figure 11. Dimensionless depth-averaged Reynolds-stress, $-(\overline{u'v'})_d/U_s^2$ (×100), across the mixing layer. All cases with $D_r \sim 0.2$ at LNEC.

Reynolds-stress, $-\overline{(u'v')}_d/U_s^2$ for the five cases considered.

Figure 10 highlights that, for the same D_r-value, the shape of the velocity profile can strongly differ depending on the direction of transverse flow. Case +38% features convex velocity profiles (Figure 10b), while the profiles of case −19% feature an inflection point (Figure 10a). This difference can be observed until $x/B_f = 10.7$, where both flow depth and velocity ratio are very similar for the five cases (Figure 2).

The existence of an inflection point in the velocity profile is a necessary condition so that Kelvin-Helmholtz instabilities turn into 2-D large coherent structures (Rayleigh's criterion) [see e.g., *Huerre and Rossi*, 1998]. In the present case, run +38% features very low levels of Reynolds-stress in comparison with the levels of run −19% (Figures 11d and 11a, respectively). Regarding the other cases, the uniform flow features an inflection point velocity profile (Figure 3g) and high levels of Reynolds-stress (Figure 11b), while case +19% (velocity not shown) and case +53% (Figure 3g) with convex velocity profiles are characterized by a poorly developed shear layer turbulence. We can thus infer that there is a strong link between the peak levels of dimensionless Reynolds-stress and the shape of mean velocity profile.

We can conclude that with a significant transverse flow to the MC (cases +38% and +53%), the Rayleigh's criterion is not fulfilled owing to the convex shape of the velocity profile, and quasi-2-D structures cannot form at the interface (see Figure 4). This results in very low levels of dimensionless Reynolds-stress. By contrast, in the presence of a clear inflectional instability, the peak levels of dimensionless Reynolds-stress are significantly increased by the quasi-2-D structures (Figure 4). This is a general result, observed for the 25 cases investigated, based on the power density spectra and temporal autocorrelation functions of velocity fluctuation.

Lastly, when the flow is nonuniform, the shape of velocity profile can be related to the momentum exchange (section 5.1.1, Figures 7 and 8). With a significant transverse flow to the MC, the momentum flux by turbulent mixing $-\rho\overline{(u'v')}_d$ is negligible compared with the momentum exchange by transverse flow $-\rho U_d V_d$. Near the interface, the MC flow is decelerated by slower water coming from the FP, resulting in a convex velocity profile in the MC. With a transverse flow to the FP, $-\rho\overline{(u'v')}_d$ is no longer negligible (Figure 7) owing to the presence of quasi-2-D structures. In addition, the fluxes $-\rho U_d V_d$ and $-\rho\overline{(u'v')}_d$ are of the same sign, both contributing to the acceleration of the FP flow and resulting in velocity profiles with an inflection point (see all cases −19% in Figure 3).

5.2. Velocity Ratio

In this section, we first analyze the effect of velocity ratio or dimensionless shear that is imposed upstream λ ($x = 0$) on the initial development of mixing layer. Second, we investigate the flow far from the inlet section, focusing on the effect of local velocity ratio $\lambda(x)$ on shear layer turbulence. Lastly, we analyze the flow features in the case of very small values of $\lambda(x)$.

5.2.1. Initial Development of the Mixing Layer

The effect of the initial conditions on the streamwise development of mixing layers was thoroughly examined in the case of free mixing layers. The latter were found to be sensitive to the geometry of the splitter-plate, to the initial laminar or turbulent boundary layer [*Bell and Mehta*, 1990], to the splitter-plate wake [*Mehta*, 1991], and to the initial value of dimensionless shear λ. If $\lambda \ll 1$, the convection velocity of structures is much larger than the velocity difference between the ambient streams, and the mixing layer development is very slow. By contrast, with an increasing λ-value, roll-up and pairings of corotating vortices start closer and closer to the splitter-plate trailing edge [*Winant and Browand*, 1974]. This results in an initial growing rate of the mixing layer width, $d\delta/dx$ ($x = 0$), proportional to $\lambda(x = 0)$ for self-preserving mixing layers [see e.g., *Yule*, 1972; *Oster and Wygnanski*, 1982].

Here the effect of $\lambda(x = 0)$ was first assessed for uniform flows (Figure 6b). At LMFA, to give more information on the near-field development, the data from *Peltier et al*. [2013a] are used. The latter data show that the initial mixing layer growing rate increases with the near-field value of λ. For instance, at $x/B_f = 1.9$, $d\delta/dx = 0.093$ and $\lambda = 0.51$ for $D_r \sim 0.2$, while $d\delta/dx = 0.056$ and $\lambda = 0.17$ for $D_r \sim 0.4$. Unlike free mixing layers, $d\delta/dx$ is not proportional to λ. However, similarly to free mixing layers, a strong initial dimensionless shear promotes a large mixing layer width, which in turn increases the mixing of the two merging flows.

When the flow is nonuniform, comparable results were obtained, as e.g., for cases −19%, +19%, and +38% with $D_r \sim 0.3$ at LMFA (Figure 6a). In the first measuring section, $\lambda = 0.41$, 0.19, and 0.13 for cases −19%, +19%, and +38%, respectively. From this plot and all the values of δ/h_f given in Table 1, we can infer that, in each flume and for a given relative depth D_r, the initial growing rate $d\delta/dx$ ($x = 0$) increases with λ ($x = 0$).

5.2.2. Far From the Inlet Section

We also investigated the effect of local dimensionless shear $\lambda(x)$ on shear layer turbulence far from the inlet section. Figure 12 shows the peak value of dimensional depth-averaged Reynolds-stress Max $[-\rho\overline{(u'v')}_d](x)$, across the two last measuring sections in both flumes, as a function of the $\lambda(x)$-value.

In each flume and for a fixed relative depth D_r, Max $[-\rho\overline{(u'v')}_d](x)$ globally increases with $\lambda(x)$. The same results are obtained when considering the peak values of local Reynolds-stress Max $[-\rho\overline{u'v'}](x)$ across the section (not shown here), showing that the previous results are not a consequence of the depth-averaging procedure. In addition, a sharp increase in Max $[-\rho\overline{(u'v')}_d]$ can be observed when λ is higher than approximately 0.3. This rise is due to a change in the turbulence structure inside the mixing layer, with the appearance of quasi-2-D structures (black-faced markers are used to indicate the presence of those structures). For the whole data set, they were detected from the power density spectra S_{yy} and autocorrelation functions R_{yy} of transverse velocity fluctuation, as carried out in section 4.2.

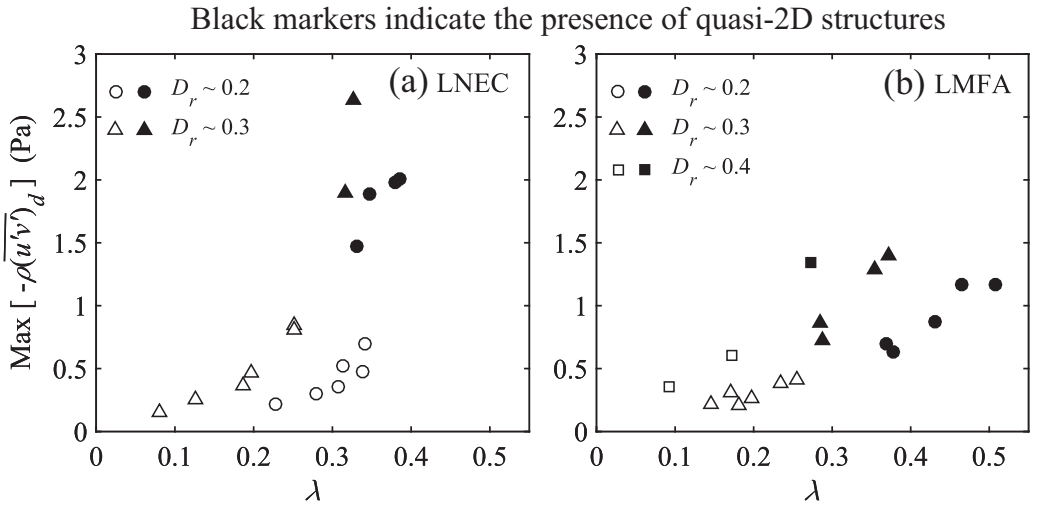


Figure 12. Peak depth-averaged Reynolds-stress Max $[-\rho\overline{(u'v')}_d]$ across the section at a given downstream position x/B_f, as a function of local dimensionless shear λ (x/B_f), for various relative depths D_r. Measurements at (a) $x/B_f = 7.1$ and 10.7 at LNEC and (b) $x/B_f = 5.6$ and 8.1 at LMFA.

As a result, the appearance of quasi-2-D structures leads to a significant rise in both dimensionless (Figure 11) and dimensional peak Reynolds-stresses (Figure 12). As shown in Figure 7, the effect of these structures at the MC/FP interface on the relative weight of Reynolds-stress $-\rho\overline{(u'v')}_d$ (compared with the transverse flow flux $-\rho U_d V_d$) in the momentum exchange is also noticeable.

5.2.3. Effect of Small Velocity Ratio

A last effect of λ can be highlighted in case where λ-values are very small along the flume. Flows with small λ-values are associated with a velocity dip in the lateral profile of depth-averaged streamwise velocity, along with a change in the sign of $-\rho\overline{(u'v')}_d$ (see Figures 3e and 3f, case +53% with $D_r \sim 0.4$ at LMFA). This dip is also observed for cases +19% and +38% (not shown in Figure 3). Regarding the λ-value, $\lambda = 0.09$ at $x/B_f = 5.6$ for case +19% (Table 1). For cases +38% and +53%, velocity difference U_s tends to zero and λ cannot be defined.

Several physical explanations to this velocity dip can be found in the literature of shear flows. In the experiments of *Stocchino and Brocchini* [2010], the dip is related to the FP "sidewall-adherence induced shearing" that rises with D_r and induces macrovortices rotating anticlockwise near the right-hand side MC/FP interface. *Nezu et al*. [1999] observed this velocity dip for a very deep uniform compound channel flow ($D_r = 0.66$), which is related to two counterrotating secondary currents that bring upward slow momentum water at the MC/FP interface. A velocity dip was observed by *Constantinescu et al*. [2011] for two flows merging at a river confluence with a λ-value close to 0. The dip is caused by the wake generated by the confluence, and the mixing layer is said to be in the "wake-mode." Similarly, such a velocity deficit was also observed by *Mehta* [1991] for free mixing layers and was attributed to the effect of the splitter-plate wake as the λ-value is lower than 0.18.

Here cases +19 to +53% with $D_r \sim 0.4$ that feature a velocity dip are associated with a significant transverse flow toward the MC. In this case, the momentum exchange is essentially driven by the transverse flow (Figure 8). The observed velocity dips can therefore not be ascribed to secondary currents or quasi-2-D macrovortices. The remaining cause is thus a lasting influence of the splitter-plate wake (deficit in streamwise mean flow) as observed by *Mehta* [1991], when λ is very low or cannot even be defined.

5.3. Vertical Confinement

The effect of relative depth D_r on the turbulent mixing layer is twofold. First, the topographical forcing by the two-stage geometry rises with a decreasing D_r-value The topographical forcing can enable shear layer turbulence to be self-sustained [*Jirka*, 2001], unlike the shallow mixing layers in single rectangular open-channels investigated by *Chu and Babarutsi* [1988], *Chu et al*. [1991], and *Uijttewaal and Booij* [2000]. In addition, the cross-flow change in flow depth is responsible for the generation of 2-D macrovortices, as investigated by *Bühler and Jacobson* [2001], *Piattella et al*. [2006], and *Pratt* [1983] in the scope of vortices dynamics in oceans, and by *Soldini et al*. [2004] in the case of uniform compound channel flows. Second, the cross-sectional development of shear layer turbulence cannot happen similarly in the three directions of space, owing to the reduced flow depth compared to the two horizontal length scales.

As previously stated, when the flow is uniform, there is an unequivocal link between (i) the shape of velocity profile or the number of interfacial macrovortices and (ii) relative depth D_r [*Stocchino and Brocchini*, 2010]. For the present nonuniform flows, this link does not exist and the effect of D_r will therefore be significantly different.

Here a first effect of D_r can be observed in Figure 12. In each flume, for a fixed λ-value, Max $[-\rho\overline{(u'v')}_d]$ increases with D_r. This result is independent of the uniformity/nonuniformity of flow. Confinement has therefore an inhibiting effect on the peak levels of shear layer turbulence.

A second effect of D_r can be observed in Figure 13, which shows the cross-sectional distribution of $-\overline{u'v'}/U_s^2$ at $x/B_f = 5.6$ in LMFA, for cases −19% with $D_r \sim 0.3$ (Figure 13a) and $D_r \sim 0.4$ (Figure 13b). While the value of λ or U_s is larger with $D_r \sim 0.3$ than with $D_r \sim 0.4$, the transverse extent of turbulent lateral shear is smaller in the shallower case. As a result, confinement is also found to have a constraining effect on the transverse development of turbulent quantities.

Confinement has actually a stronger constraining effect on shear layer turbulence when the latter is essentially 3-D, than when turbulence is driven by quasi-2-D structures. This will be shown in Figure 14, where is plotted the peak dimensionless depth-averaged Reynolds-stress Max $[-\overline{(u'v')}_d/U_s^2]$ across the two last

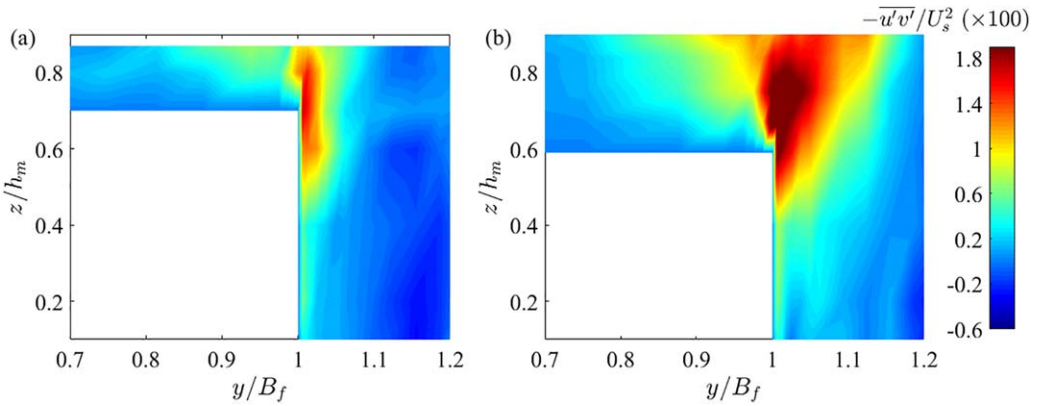


Figure 13. Distribution of dimensionless Reynolds-stress $-\overline{u'v'}/U_s^2$ (×100) at downstream position $x/B_f = 5.6$ at LMFA. Cases −19% with (a) $D_r \sim 0.3$ and λ ($x/B_f = 5.6$) = 0.35 and (b) $D_r \sim 0.4$ and λ ($x/B_f = 5.6$) = 0.27.

measuring sections in each flume, as a function of local λ-value. Figures 14a and 14b refer to LMFA and LNEC, respectively. Also shown in Figure 14b are the data for free mixing layers and for shallow mixing layers in a single rectangular open-channel (references in the figure caption). Data from *Fernandes et al.* [2014] for uniform compound channel flows at LNEC with $D_r \sim 0.10$, 0.15, 0.25, and 0.38 are also reported in Figure 14b. In the presence of quasi-2-D structures (evidence provided by spectra S_{yy} and autocorrelation function R_{yy}), the flow cases are surrounded by an ellipse in both figures. Note that with data from

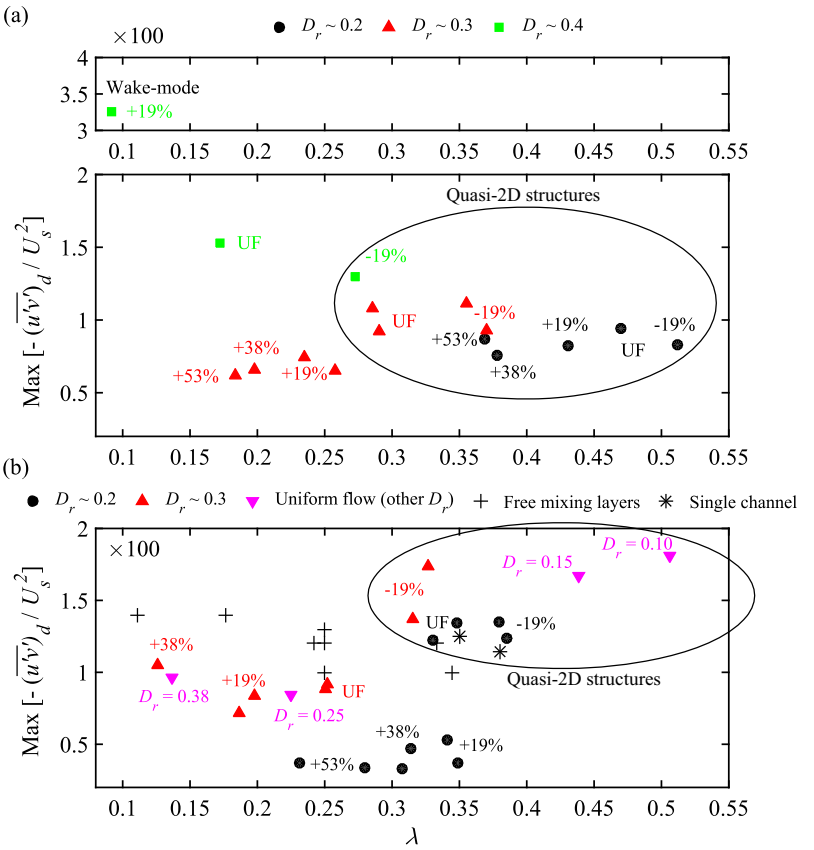


Figure 14. Peak Reynolds-stress Max$[-(\overline{u'v'})d/U_s^2]$ across the two last measuring sections in each flume against local λ-value at (a) LMFA, present data and (b) LNEC, present data and uniform flows of *Fernandes et al.* [2014] with $D_r \sim 0.10$, 0.15, 0.25, and 0.38. Are also reported in Figure 14b data for free mixing layers after *Oster and Wygnanski* [1982], *Mehta* [1991], *Bell and Mehta* [1990], *Yule* [1972], *Loucks and Wallace* [2012], and data for shallow mixing layers in a single channel [*Uijttewaal and Booij*, 2000].

Fernandes et al. [2014], the spectra S_{yy} features quasi-2-D structures for $D_r \sim 0.10$ and 0.15, and only 3-D turbulence with $D_r \sim 0.25$ and 0.38 (spectra not shown here).

The results first show that the effect of D_r on Max $[-\overline{(u'v')}_d/U_s^2]$ is significant when $\lambda \leq 0.3$ and in absence of quasi-2-D structures. For instance, Max $[-\overline{(u'v')}_d/U_s^2]$ is far lower for $D_r \sim 0.3$ than for $D_r \sim 0.4$ at LMFA (Figure 14a). By contrast, as $\lambda \geq 0.3$ and in the presence of quasi-2-D macrovortices, the effect of D_r is less important or can vanish. The results are noticeable at LNEC (Figure 14b), since the values of Max $[-\overline{(u'v')}_d/U_s^2]$ are very high, while the D_r-value ranges from 0.10 to 0.3. In addition, the highest values are obtained for the shallowest case, the uniform flow with $D_r \sim 0.10$. Very high dimensionless shears ($\lambda \geq 0.5$) can thus trigger the development of quasi-2-D structures, irrespective of their confinement. Following *Uijttewaal* [2014], we can state that 3-D bed-generated turbulence and quasi-2-D macrovortices do not interact significantly for these flow cases. This leads to very high levels of dimensionless Reynolds-stresses that can be higher than the upper levels observed for free mixing layers.

This variation in the confinement effect depending on the presence or absence of quasi-2-D macrovortices can also be observed on the width-to-depth ratio δ/h_f. For instance at LMFA (see Table 1), $\delta/h_f = 15.8$ for the uniform flow with $D_r \sim 0.2$ and with quasi-2-D structures (case denoted "UF" in Figure 14a), while $\delta/h_f = 2.6$ for a uniform flow with $D_r \sim 0.4$ without quasi-2-D structures.

We can thus conclude that the confinement effect on shear layer turbulence is more effective for weakly sheared flows than for highly sheared flows, irrespective of uniformity/nonuniformity of flow.

Lastly, case +19% with $D_r \sim 0.4$ at LMFA (Figure 14a) must be excluded from the analysis. This run is in the "wake-mode" [*Constantinescu et al*., 2011] owing to the dip in the velocity profile (not shown, similar to case +53% in Figure 3e), resulting in the highest value of Max $[-\overline{(u'v')}_d/U_s^2]$ equals to 3.25×10^{-2} with $\lambda = 0.09$ (Table 1). This value is comparable to those measured by *Mehta* [1991] for free mixing layers influenced by the splitter-plate wake (e.g., 3.5×10^{-2} with $\lambda = 0.1$).

6. Conclusion

This experimental study assessed the effects of three forcings on mixing layers and quasi-2-D coherent structures in compound channels: (a) a transverse depth-averaged mean flow (termed "transverse flow"); (b) a variable local velocity ratio or dimensionless shear $\lambda(x)$; and (c) a variable flow confinement quantified by relative flow depth D_r. The main findings are listed below:

The effect of transverse flow depends upon its direction and magnitude:

1. With a significant transverse flow toward the main channel (MC), shear layer turbulence cannot develop over the floodplain (FP). As turbulence is essentially located in the MC, this prevents any exchange of pollutants, nutrients, or sediments from MC to FP. Momentum exchange is driven by the transverse flow (negligible contributions of turbulent mixing and secondary currents). This results in convex mean velocity profiles in the MC, as slower water from the FP enters the faster MC flow. The Rayleigh's criterion is not fulfilled, and quasi-2-D structures cannot develop at the MC/FP interface. Their absence induces low peak levels of dimensional (Max $[-\rho\overline{(u'v')}_d]$) and dimensionless (Max $[-\overline{(u'v')}_d/U_s^2]$) depth-averaged Reynolds-stresses, and a small and fairly constant mixing layer width δ.
2. With a transverse flow toward the FP, Reynolds-stresses, secondary currents and transverse flow all contribute to momentum exchange. Over the FP, the flow is accelerated by the turbulent mixing and transverse flow, resulting in a marked inflectional instability in the mean velocity profile along with quasi-2-D structures. The dimensional and dimensionless peak Reynolds-stresses are high and width δ increases toward downstream.

The effect of velocity ratio λ is threefold:

1. A high initial value of λ promotes a high growing rate of δ, and high levels of Reynolds-stress in the whole measuring domain, irrespective of uniformity/nonuniformity of flow (i.e., of transverse flow).
2. Far from the inlet section, the peak value Max $[-\rho\overline{(u'v')}_d]$ across a given section increases with local λ-value for a fixed D_r-value.
3. A λ-value ≥ 0.3 was found to be a necessary condition to the development of quasi-2-D structures, whose appearance results in a sharp increase in Max $[-\rho\overline{(u'v')}_d]$ and Max $[-\overline{(u'v')}_d/U_s^2]$. The latter can

be higher than those observed for free mixing layers or shallow mixing layers in a single rectangular channel.

Regarding the confinement effect:

1. Unlike uniform compound channel flows, there is no unequivocal link between D_r and velocity difference $U_s = (U_{d2} - U_{d1})$ or velocity ratio λ for nonuniform flows. As a result, the existence of quasi-2-D structures was found to be independent of D_r, as their development is controlled by the λ-value, and by the direction and magnitude of transverse flow.
2. By contrast, confinement can have a constraining effect on the transverse development of shear layer turbulence and can reduce peak dimensional and dimensionless Reynolds-stresses. This effect is important for weakly sheared flows (λ-value < 0.3) for which turbulence is essentially 3-D. However, no effect was observed for highly sheared flows (λ-value > 0.5) driven by the quasi-2-D structures.

This study clearly pointed out that in compound channels, the transverse flow existing in a streamwise nonuniform flow (the most common real situation) could significantly alter turbulent flow structure when compared to uniform flow conditions, with practical implications for river engineering studies. Moreover, this study showed that both velocity ratio and transverse flow control the formation of quasi-2-D structures, besides the two-stage geometry. The latter result may be important for CFD modeling, since anisotropic turbulence models (at least) or large-eddy simulations will be required in the presence of these structures.

Notations

B	total width.
B_i	subsection width.
D_r	relative flow depth.
f	signal frequency.
g	gravitational acceleration constant.
h_b	bank full stage in the main channel.
h_f	flow depth in the floodplain.
h_m	flow depth in the main channel (outside the sloping bank area at LNEC).
k	wave number ($2\pi f/U$).
N	nonuniformity parameter (λ / λ^u).
Q	total discharge.
Q_i	subsection discharge.
Q_f^u	floodplain discharge under uniform flow conditions.
$\Delta Q_f/Q_f^u$	variation in floodplain inflow with respect to Q_f^u.
R_e	Reynolds number.
S_0	longitudinal bed slope.
S_{fi}	subsection friction slope.
u, v, w	instantaneous streamwise, transverse, and vertical velocities.
U, V, W	time-averaged streamwise, transverse and vertical velocities.
u', v', w'	fluctuations about the time-averaged velocities ($u = U + u'$).
U_c	average velocity across the mixing layer ($U_{d2} + U_{d1}$)/2.
U_d	depth-averaged mean streamwise velocity.
U_{d1}	depth-averaged mean streamwise velocity of the low speed ambient stream.
U_{d2}	depth-averaged mean streamwise velocity of the high speed ambient stream.
U_{int}	depth-averaged mean streamwise velocity at the main channel/floodplain interface.
U_s	velocity difference between the two ambient streams ($U_{d2}- U_{d1}$).
V_d	depth-averaged mean transverse velocity.
x, y, z	longitudinal, lateral and vertical directions.
$\bar{y}$	center of the mixing layer.
δ	mixing layer width.
ρ	water density.
$-\rho\left(\overline{u'v'}\right)$	local Reynolds-stress.
$-\rho\left(\overline{u'v'}\right)_d$	depth-averaged Reynolds-stress.

λ velocity ratio or dimensionless shear $(U_{d2} - U_{d1})/(U_{d1} + U_{d2})$.
λ^u velocity ratio under uniform flow conditions.
Λ_x streamwise integral length scale of coherent structure.
ν kinematic viscosity of water.

Subscripts

f concerning floodplain.
i concerning a subsection.
m concerning main channel.
d refers to a depth-averaged value.

Acknowledgments
Travel costs of J. B. Leal, J. N. Fernandes, and S. Proust were supported by two projects: a Hubert Curien Project Pessoa, funded by EGIDE, France and by FCT, Portugal; and the FlowRes ANR project funded by the French National Research Agency under grant N° ANR-14-CE03-0010. J. N. Fernandes acknowledges the support of the Portuguese Science and Technology Foundation through the grant SFRH/BPD/114768/2016. The authors thank Fabien Thollet, Mickaël Lagouy, and Pedro Duarte for their assistance during the experiments. The authors also thank the anonymous reviewers for their valuable comments and suggestions to improve the quality of the paper. S. Proust thanks V. Dupuis for his critical analysis of the results. The experimental data could be downloaded by the end of 2017 on the FlowRes website: http://flowres.irstea.fr/en/.

References

Bell, J. H., and R. D. Mehta (1990), Development of a two-stream mixing layer from tripped and untripped boundary layers, *AIAA J.*, *28*(12), 2034–2042.
Besio, G., A. Stocchino, S. Angiolani, and M. Brocchini (2012), Transversal and longitudinal mixing in compound channels, *Water Resour. Res.*, *48*, W12517, doi:10.1029/2012WR012316.
Bousmar, D., N. Wilkin, J. H. Jacquemart, and Y. Zech (2004), Overbank flow in symmetrically narrowing floodplains, *J. Hydraul. Eng.*, *130*(4), 305–312.
Bousmar, D., N. Rivière, S. Proust, A. Paquier, R. Morel, and Y. Zech (2005), Upstream discharge distribution in compound-channel flumes, *J. Hydraul. Eng.*, *131*(5), 408–412.
Bousmar, D., S. Proust, and Y. Zech (2006), Experiments on the flow in a enlarging compound channel, paper presented at International Conference on Fluvial Hydraulics, River Flow 2006, Lisbon, 6–8 Sept., edited by Ferreira, Alves, Leal and Cardoso , Taylor & Francis Group, London.
Bühler, O., and T. E. Jacobson (2001), Wave-driven currents and vortex dynamics on barred beaches, *J. Fluid Mech.*, *449*, 313–339.
Chu, V. H., and S. Babarutsi (1988), Confinement and bed-friction effects in shallow turbulent mixing layers, *J. Hydraul. Eng.*, *114*(10), 1257–1274.
Chu, V. H., J. H. Wu, and R. E. Khayat (1991), Stability of turbulent shear flows in shallow open channels, *J. Hydraul. Eng.*, *117*(10), 1370–1388.
Constantinescu, G., S. Miyawaki, B. Rhoads, A. Sukhodolov, and G. Kirkil (2011), Structure of turbulent flow at a river confluence with momentum and velocity ratios close to 1: Insight provided by an eddy-resolving numerical simulation, *Water Resour. Res.*, *47*, W05507, doi:10.1029/2010WR010018.
Dracos, T., M. Giger, and G. H. Jirka (1992), Plane turbulent jets in a bounded fluid layer, *J. Fluid Mech.*, *241*, 587–614.
Dupuis, V., S. Proust, C. Berni, and A. Paquier (2017a), Mixing layer development in compound channel flows with submerged and emergent rigid vegetation over the floodplains, *Exp. Fluids*, *58*, 30, doi: 10.1007/s00348-017-2319-9.
Dupuis, V., S. Proust, C. Berni, and A. Paquier (2017b), Compound channel flow with a longitudinal transition in hydraulic roughness over the floodplains, *Environ. Fluid Mech.*, 1–26, doi:10.1007/s10652-017-9525-0.
Elliot, S. C. A., and R. H. J. Sellin (1990), SERC Flood channel facility: Skewed flow experiments, *J. Hydraul. Res.*, *28*(2), 197–214.
Fernandes, J. N., J. B. Leal, and A. H. Cardoso (2014), Improvement of the Lateral Distribution Method based on the mixing layer theory, *Adv. Water Resour.*, *69*, 159–167.
Goring, D. G., and V. Nikora (2002), Despiking acoustic Doppler velocimeter data, *J. Hydraul. Eng.*, *128*(1), 117–126.
Han, L., E. Mignot, and N. Rivière (2016), Shallow mixing layer downstream from a sudden expansion, *J. Hydraul. Eng.*, *143*(5), doi:10.1061/(ASCE)HY.1943-7900.0001274.
Huerre, P., and M. Rossi (1998), Hydrodynamic instabilities in open flows, in *Hydrodynamics and Nonlinear Instabilities*, edited by C. Godrèche and P. Manneville, pp. 81–294, Cambridge Univ. Press, New York.
Jirka, G. H. (2001), Large scale flow structures and mixing processes in shallow flows, *J. Hydraul. Res.*, *39*(6), 567–573.
Knight, D. W., and K. Shiono (1990), Turbulence measurements in a shear layer region of a compound channel, *J. Hydraul. Res.*, *28*(2), 175–194.
Kraichnan, R. H. (1967), Inertial ranges in two-dimensional turbulence, *Phys. Fluids*, *10*(7), 1417–1423.
Lesieur, M. (1997), *Turbulence in Fluids*, 3rd rev. enlarged ed., 515 pp., Kluwer Acad., Dordrecht, The Netherlands.
Lindborg, E. (1999), Can the atmosphere kinetic energy spectrum be explained by two-dimensional turbulence?, *J. Fluid Mech.*, *388*, 259–288.
Loucks, R. B., and J. M. Wallace (2012), Velocity and velocity gradient based properties of a turbulent plane mixing layer, *J. Fluid Mech.*, *699*, 280–319.
McLelland, S. J., and A. P. Nicholas (2000), A new method for evaluating errors in high-frequency ADV measurements, *Hydrol. Processes*, *14*(2), 351–366.
Mehta, R. D. (1991), Effect of velocity ratio on plane mixing layer development: Influence of the splitter plate wake, *Exp. Fluids*, *10*, 194–204.
Nezu, I., K. Onitsuka, and K. Iketani (1999), Coherent horizontal vortices in compound open channel flows, in *Hydraulic Modeling*, edited by I. W. Seo, J. H. Sonu, and V. P. Singh, pp. 17–32, Water Resour. Publ., Colo.
Oster, D., and I. Wygnanski (1982), The forced mixing layer between parallel streams, *J. Fluid Mech.*, *123*, 91–130.
Peltier, Y., S. Proust, N. Rivière, A. Paquier, and K. Shiono (2013a), Turbulent flows in straight compound open-channel with a transverse embankment on the floodplain, *J. Hydraul. Res.*, *51*(4), 446–458.
Peltier, Y., N. Rivière, S. Proust, E. Mignot, A. Paquier, and K. Shiono (2013b), Estimation of the error on the mean velocity and on the Reynolds stress due to a misoriented ADV probe in the horizontal plane: Case of experiments in a compound open-channel, *Flow Meas. Instrum.*, *34*, 34–41.
Piattella, A., M. Brocchini, and A. Mancinelli (2006), Topographically controlled, breaking-wave-induced macrovortices: Part 3. The mixing features, *J. Fluid Mech.*, *559*, 81–106.
Pope, S. B. (2000), Free shear flows, in *Turbulent Flows*, pp. 139–144, Cambridge Univ. Press, New York.
Pratt, L. J. (1983), On inertial flow over topography. Part 1. Semigeostrophic adjustment to an obstacle, *J. Fluid Mech.*, *131*, 195–218.

Proust, S. (2005), Ecoulements non-uniformes en lits composés: effets de variations de largeur du lit majeur, PhD thesis, 362 pp., INSA de Lyon, Lyon, France.
Proust, S., N. Rivière, D. Bousmar, A. Paquier, Y. Zech, and R. Morel (2006), Flow in compound channel with abrupt floodplain contraction, *J. Hydraul. Eng.*, *132*(9), 958–970.
Proust, S., D. Bousmar, N. Rivière, A. Paquier, and Y. Zech (2009), Nonuniform flow in compound channel: A 1-D method for assessing water level and discharge distribution, *Water Resour. Res.*, *45*, W12411, doi:10.1029/2009WR008202.
Proust, S., D. Bousmar, N. Rivière, A. Paquier, and Y. Zech (2010), Energy losses in compound open channels, *Adv. Water Resour.*, *33*, 1–16.
Proust, S., J. N. Fernandes, Y. Peltier, J. B. Leal, N. Rivière, and A. H. Cardoso (2013), Turbulent non-uniform flows in straight compound open-channels, *J. Hydraul. Res.*, *51*(6), 656–667.
Rutgers, M. (1998), Forced 2D turbulence: Experimental evidence of simultaneous inverse energy and forward enstrophy cascades, *Phys. Rev. Lett.*, *81*(11), 2244.
Sellin, R. H. J. (1964), A laboratory investigation into the interaction between the flow in the channel of a river and that over its flood plain, *La Houille Blanche*, *7*, 793–802.
Shiono, K., and D. W. Knight (1991), Turbulent open channel flows with variable depth across the channel, *J. Fluid Mech.*, *222*, 617–646.
Shiono, K., and Y. Muto (1998), Complex flow mechanisms in compound meandering channels with overbank flow, *J. Fluid Mech.*, *376*, 221–226.
Soldini, L., A. Piattella, A. Mancinelli, R. Bernetti, and M. Brocchini (2004), Macrovortices-induced horizontal mixing in compound channels, *Ocean Dyn.*, *54*(3), 333–339.
Stocchino, A., and M. Brocchini (2010), Horizontal mixing of quasi-uniform straight compound channel flows, *J. Fluid Mech.*, *643*, 425–435.
Stocchino, A., G. Besio, S. Angiolani, and M. Brocchini (2011), Lagrangian mixing in straight compound channels, *J. Fluid Mech.*, *675*, 168–198.
Tominaga, A., and I. Nezu (1991), Turbulent structure in compound open-channel flows, *J. Hydraul. Eng.*, *117*(1), 21–41.
Uijttewaal, W. S. J. (2014), Hydrodynamics of shallow flows: Application to rivers, *J. Hydraul. Res.*, *52*(2), 157–172.
Uijttewaal, W. S. J., and R. Booij (2000), Effects of shallowness on the development of free-surface mixing layers, *Phys. Fluids*, *12*(2), 392–420.
Vermaas, D. A., W. S. J. Uijttewaal, and A. J. F. Hoitink (2011), Lateral transfer of streamwise momentum caused by a roughness transition across a shallow channel, *Water Resour. Res.*, *47*, W02530, doi:10.1029/2010WR010138.
Winant, C. D., and F. K. Browand (1974), Vortex pairing: The mechanism of turbulent mixing-layer growth at moderate Reynolds number, *J. Fluid Mech.*, *63*, part 2, 237–255.
Yule, A. J. (1972), Two dimensional self-preserving turbulent mixing layers at different free stream velocity ratios, *Aeronaut. Res. Counc. Rep. Memo. 3683*, Dep. of the Mech. of Fluids, Univ. of Manchester, HM Stationery Office, London.